

EFFECTS OF BEND-TWIST COUPLING DEFORMATION ON THE AERODYNAMIC PERFORMANCE OF A WIND TURBINE BLADE

Nawapon Sompong and *Pongtorn Prombut

Faculty of Engineering, Kasetsart University, Thailand

*Corresponding Author, Received: 30 June 2016, Revised: 10 August 2016, Accepted: 30 Nov. 2016

ABSTRACT: Comprehensive research exists on passive pitch control of wind turbines using bend-twist coupling property of composite materials. Blades with bend-twist coupling deformation can increase energy capture, improve dynamic stability, or reduce aerodynamic loads. The objectives of this work are to apply bend-twist coupling into an existing blade design and to investigate the resulting aerodynamic performance. The 41.25-meter blade was based on GE 1.5 GLX wind turbine. Aerodynamic loads were calculated using Blade Element Momentum (BEM) theory and Computational Fluid Dynamics (CFD) simulation. The resultant thrust and torque from both methods agree well. However, only the CFD can provide details of pressure distribution over the complex blade surface. Three levels of bend-twist coupling were designed for the Glass/Epoxy blade skins i.e. no coupling, low coupling, and high coupling. From Finite Element Analysis (FEA), the deflections of the three blades were slightly different while the twist angles were considerably different. The deformed geometries of the blades were then used to produce new three dimensional (3D) models for the prediction of the power coefficient (C_p) by CFD. The results show that the proper bend-twist coupling laminate can improve the performance of the blade. At low wind speed, the C_p is higher than the baseline blade. At wind speed greater than rated speed, however, the blades twist too much and the C_p decreases below the baseline blade. Simulation of 3D blade models can help in the design of a bend-twist coupling level suitable to the blade shape and wind speed.

Keywords: Wind Turbine, Bend-Twist Coupling, Composite Materials, Power Coefficient

1. INTRODUCTION

Wind turbines operate in uncertain wind conditions both in terms of speed and direction. Yawing mechanism is used to maintain the rotor plane normal to the wind direction. Pitch adjustment is used to achieve optimum angle of attack of the blade in varying wind speed. Comprehensive research exists on passive pitch control of wind turbines using bend-twist coupling property of composite materials. Blades with bend-twist coupling deformation can increase energy capture, improve dynamic stability, or reduce aerodynamic loads. Lobitz et al. [1] found that, for a blade that twists 2 degrees toward stall, the annual energy production can increase by 10-15%. The twist behavior was created as a function and was prescribed into the blade geometry. An investigation of bend-twist coupling in composite box-beams showed that induced twist can be produced by tip-loading on the beams [2]. Full blade Finite Element Analysis (FEA) with bend-twist coupling produced from the off-axis carbon spar caps has been studied [3]. Twisting deformation was obtained when concentrated loads were applied at 4 stations along the blade span. However, the effects of the twist on the aerodynamic performance have not been addressed. Aerodynamic-structure interaction simulation using Blade Element Momentum theory for power prediction and Finite Element (FE)-based code for blade deformation has been studied [4]. The FE part modeled a wind turbine

blade as a beam made by orthotropic materials and optimized it with Genetic Algorithm-based tools to achieve optimum power production. Mirror layups of the blade shells produced an induced twist toward stall and improved in the energy capture by 15.5%. Another Fluid-Structure Interaction approach used BEM to calculate the aerodynamic loads and used 3D FEA to predict the deformation of the blade [5]. This iterative analysis showed that the deflection of the blade reduces the power output. However, blade twist was not considered.

Passive pitch control by bend-twist coupling of wind turbine blades involves aerodynamic analysis, structural analysis, and composite structural design. Limited work has been done in all three aspects, especially on 3D blade geometries. The present work aims to produce bend-twist coupling deformation in an existing blade geometry. Full 3D blade models are used for CFD and FEA analyses. The coupling properties of composite materials produce twisting deformation as the blades bend under wind loads. The deformed geometries from FEA are assumed to be the blade shapes in operation. The second round of CFD simulation is performed to predict and compare the power coefficient of the blades with different level of bend-twist coupling.

2. LAMINATE BEND-TWIST COUPLING

The relationship between stresses and strains in

composite laminates can be described by the classical lamination theory [6]

$$\begin{Bmatrix} N_x \\ N_y \\ N_{xy} \\ M_x \\ M_y \\ M_{xy} \end{Bmatrix} = \begin{bmatrix} A_{11} & A_{12} & A_{16} & B_{11} & B_{12} & B_{16} \\ A_{12} & A_{22} & A_{26} & B_{12} & B_{22} & B_{26} \\ A_{16} & A_{26} & A_{66} & B_{16} & B_{26} & B_{66} \\ B_{11} & B_{12} & B_{16} & D_{11} & D_{12} & D_{16} \\ B_{12} & B_{22} & B_{26} & D_{12} & D_{22} & D_{26} \\ B_{16} & B_{26} & B_{66} & D_{16} & D_{26} & D_{66} \end{bmatrix} \begin{Bmatrix} \epsilon_x^0 \\ \epsilon_y^0 \\ \gamma_{xy}^0 \\ \kappa_x \\ \kappa_y \\ \kappa_{xy} \end{Bmatrix} \quad (1)$$

- [A]: Extensional stiffness matrix
- [B]: Bending-extension coupling stiffness matrix
- [D]: Bending stiffness matrix

The bend-twist coupling occurs when D_{16} and D_{26} are non-zero. These parameters relate bending moments (M_x, M_y) to twisting deformation (κ_{xy}) and twisting moment (M_{xy}) to bending deformations (κ_x, κ_y). The dimensionless parameter used to indicate the level of coupling is [7]

$$B_i = \left| \frac{D_{16}}{D_{11}} \right| \quad (2)$$

3. BLADE GEOMETRY

Geometry used for the construction of blade model is based on the technical specifications of GE 1.5 XLE wind turbine. This 41.25 m blade produces 1.5 MW in the wind speed of 10 m/s. Three airfoils are used in 20 blade stations [8] as shown in Table 1.

Table 1 Distribution of chord, twist, and shape

Station	Span (m)	Chord (m)	Twist (deg.)	Airfoil
1	3.09375	2.5328	42.00	S818
2	5.15625	2.8157	32.00	
3	7.21875	3.0740	23.00	
4	9.28125	3.2101	15.00	
5	11.34375	3.1115	11.50	
6	13.40625	2.9651	8.20	
7	15.46875	2.8182	7.00	
8	17.53125	2.6726	6.00	
9	19.59375	2.5270	5.00	S825
10	21.65625	2.3805	4.00	
11	23.71875	2.2337	4.15	
12	25.78125	2.0881	3.85	
13	27.84375	1.9146	3.25	
14	29.90625	1.7985	2.75	
15	31.96875	1.6599	1.25	
16	34.03125	1.5279	0.75	

Station	Span (m)	Chord (m)	Twist (deg.)	Airfoil
17	36.09375	1.3963	0.85	S826
18	38.15625	1.2647	0.55	
19	40.21875	1.3331	0.05	
20	41.25000	1.0000	0.00	

The airfoils are created at the specified span as shown in Fig. 1.

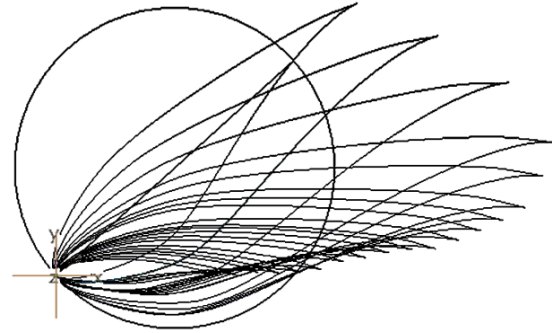


Fig. 1 Airfoils distribution along the blade span.

The blade geometry is then created using 3D surface features in a CAD program to produce the blade surfaces between the airfoils (Fig. 2).

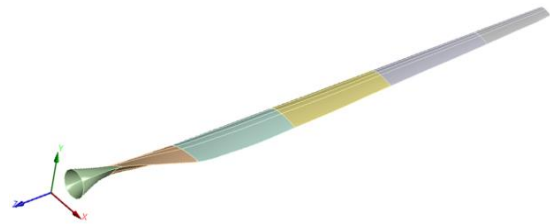


Fig. 2 Blade geometry.

4. AERODYNAMICS ANALYSIS

Determination of aerodynamic forces acting on the blade is carried out using two methods. An analytical method uses Blade Element Momentum theory and a numerical method uses Computational Fluid Dynamics simulation.

4.1 Blade Element Momentum (BEM) Theory

The BEM theory consists of Momentum theory and Blade Element theory. For the Momentum theory, energy conservation of air stream passing through the wind turbine yields an equation for the normal force (thrust, F_x) and conservation of angular momentum yields an equation for the torque (T) of an annular element of airstream [9].

$$dF_x = 4a(1 - a)\rho V_1^2 \pi r dr \quad (3)$$

$$dT = 4a'(1 - a)\rho V_1 \Omega \pi r^3 dr \quad (4)$$

where ρ is the air density, V_1 is the upstream wind velocity, Ω is the blade rotational speed, and r is the rotor radius. The Blade Element theory uses force equilibrium in each blade section to produce equations for the thrust and torque.

$$dF_x = \sigma' \pi \rho \left[\frac{V_0(1-a)}{\sin\phi} \right]^2 (C_L \cos\phi + C_D \sin\phi) r dr \quad (5)$$

$$dT = \sigma' \pi \rho \left[\frac{V_0(1-a)}{\sin\phi} \right] \left[\frac{\Omega r(1+a')}{\cos\phi} \right] (C_L \sin\phi + C_D \cos\phi) r^2 dr \quad (6)$$

where σ' is the rotor solidity, V_0 is the wind velocity, and ϕ is the inflow angle. The thrust and torque equations from Momentum theory and Blade Element theory can be matched to produce equations for the axial induction factor (a) and angular induction factor (a').

$$\frac{a}{1-a} = \frac{\sigma'}{4\sin^2\phi} (C_L \cos\phi + C_D \sin\phi) \quad (7)$$

$$\frac{a'}{1-a'} = \frac{\sigma'}{4\sin\phi\cos\phi} (C_L \sin\phi + C_D \cos\phi) \quad (8)$$

Equations (7) and (8) can be solved iteratively for a and a' . The lift and drag coefficients (C_L and C_D) are from JavaFoil [10].

The aerodynamic thrust force and torque can then be obtained by integrating Eq. (5) and (6) respectively. Additionally, the power coefficient (C_p) of the blade can be calculated with the following equation [9].

$$C_p = \frac{8}{\lambda^2} \int_{\lambda_h}^{\lambda} \lambda_r^3 a'(1-a) d\lambda_r \quad (9)$$

where λ is the tip speed ratio.

4.2 Computational Fluid Dynamics (CFD)

The CFD simulation is performed on the full blade model shown in Fig. 2. To reduce the computing resource, only one blade in a 120° domain section is modeled as shown in Fig. 3. Periodic boundary condition is used to keep the simulation equivalent to three blades in a circular-section domain. The inlet radius is 3 times the blade length and 2.5 times upstream from the blade. The outlet radius is 6 times the blade length and the distance is 4.5 times downstream from the blade. The simulation is performed using SST $k-\omega$ turbulence model. The mesh contains about 970,000 tetrahedron elements which give the non-dimensional parameter Y^+ equals 220 or the wall distance 0.01 m. The mesh orthogonal quality is more than 0.5 and the mesh skewness is less than 0.75.

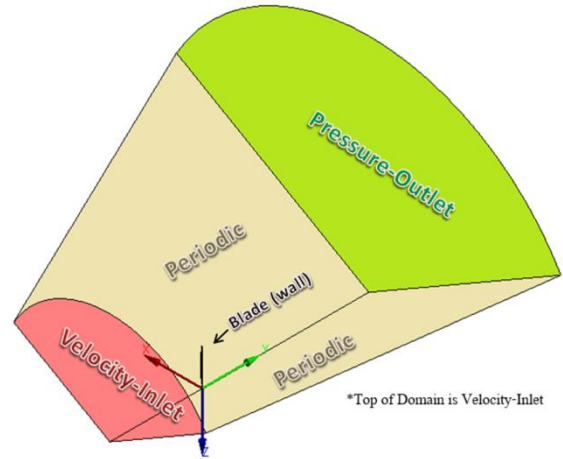


Fig. 3 CFD Model of blade, domain, and boundary

The aerodynamic loads on the undeformed blade under the wind speed of 10 m/s are presented in Table 2. The results from the BEM and CFD methods agree well. Hence, both methods can be used with confidence.

Table 2 Thrust and torque on rigid blade at 10 m/s

Aero. Load	BEM	CFD	Diff (%)
Thrust (N)	104,805	115,624	10.32
Torque (kN-m)	2,574	2,614	1.55

5. BLADE STRUCTURAL ANALYSIS

5.1 Blade Internal Structure

A blade section has a shape of an airfoil. The blade skin is divided by the chord line into upper and lower shells. A spar is used to provide bending resistance which reduces the blade deflection. The present work adopts the blade construction from Zuteck [11]. The spar caps cover from 15% to 45% of the chord. The spar web is placed at 30% of the chord as shown in Fig. 4.

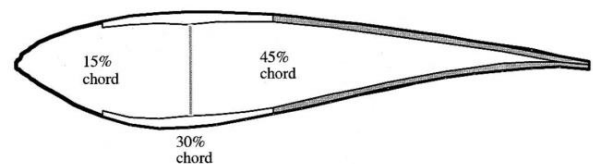


Fig. 4 Internal structure of a wind turbine blade [11]

The blade skin is modeled with E-Glass/Epoxy unidirectional (UD) composite while Carbon/Epoxy is used for the spar caps. The spar web is modeled with steel to simplify the model construction. Table 2 shows properties of the composites [12].

Table 3 Properties of UD laminae ($V_f = 60\%$)

Material	E_1 (GPa)	E_2 (GPa)	G_{12} (GPa)	ν_{12}
E-Glass/Epoxy	40	8	4	0.25
Carbon/Epoxy	135	10	5	0.30

Three sets of layups are used for the blade skin. Layup B1 is for $[0/90/0/90/0]_X$, B2 for $[20/-70/-70/20]_X$, and B3 for $[20_5]_X$, where X is the number of sets needed to attain a desired thickness. The layups are selected to produce different level of coupling. From existing literature, layup B1 does not have coupling property, layup B2 produces high extension-twist coupling [13], while layup B3 yields better bend-twist coupling [3], [4]. Using Eq. (1) and (2) with the

properties of E-Glass/Epoxy, the bend-twist coupling parameter B_t for the layups B1, B2, and B3 are 0.0000, 0.2274, and 0.2587 respectively. The layups are expected to cause different twisting deformation, thus different power production efficiency.

Figure 5 shows the thickness variation of the blade skin. The blade length is divided into 5 sections with the thickness of 30 mm, 26 mm, 22 mm, 18 mm, and 14 mm from root to tip. The E-Glass/Epoxy has the thickness of 0.2 mm/ply, therefore the Section 1 can be produced with the layup $[20/-70/-70/20]_{30}$, for example. The spar cap is made from Carbon/Epoxy with the layup of $[0/0/0/90/90/90/0/0/0]_3$. Its thickness is 6 mm throughout the blade length. An example of the laminate in the Section 1 using layup B2 is shown in Fig. 6.

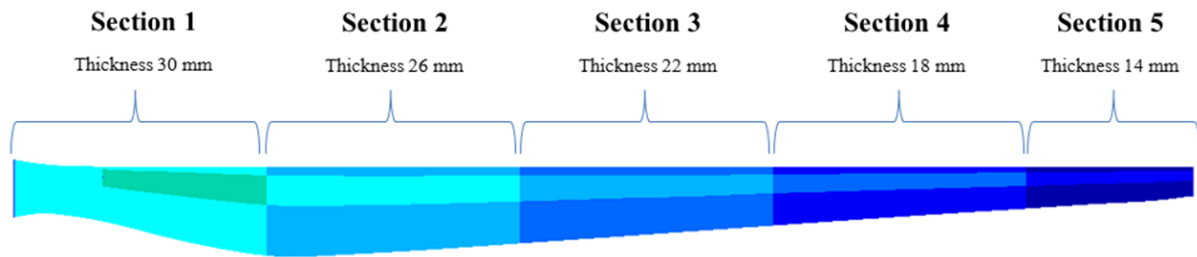


Fig. 5 Blade skin thickness along the span

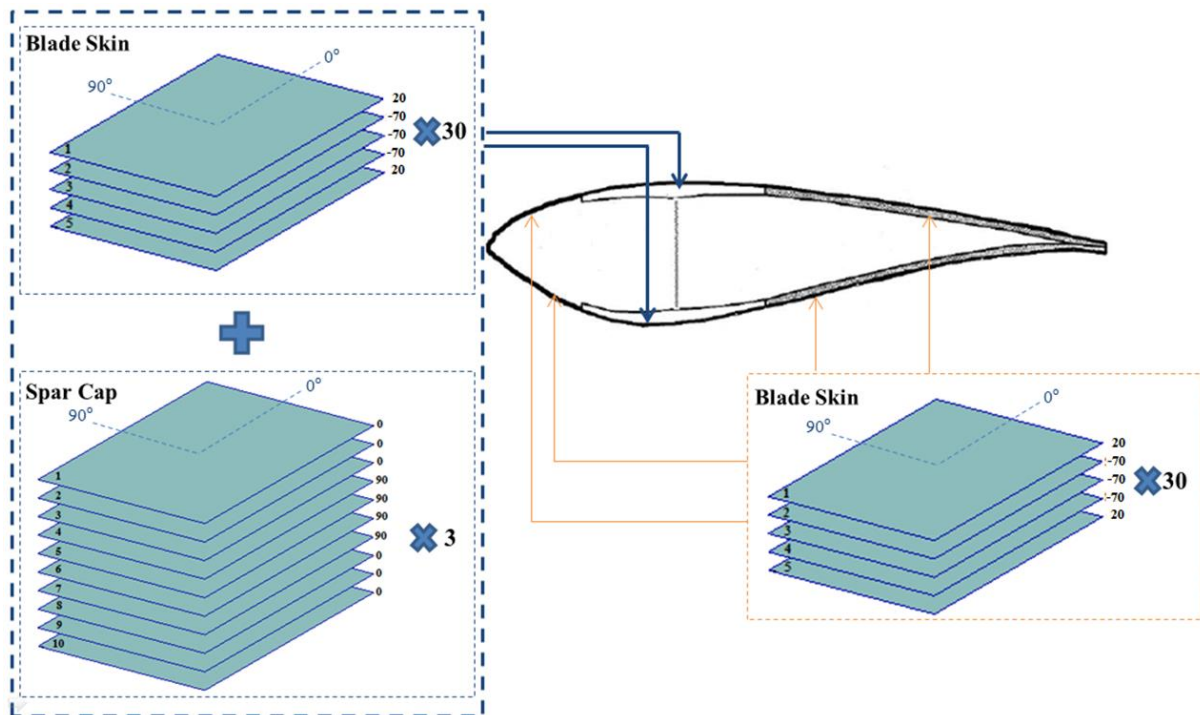


Fig. 6 Layup B2 and spar caps of blade section 1

5.2 Finite Element Analysis (FEA)

The finite element model uses the blade geometry and construction details of the preceding sections and represents the blade with 120,000 quadrilateral elements. The aerodynamic load, taken from the CFD analysis, is applied as pressure on the elements. The present work is focused on the deformation of the blade. Bending and twisting results are used to create deformed blade geometries. These new geometries assume that there is no deformation of the airfoils, the blade deflection can be represented by the displacement of the leading edge, and the twist can be represented by the rotation about the leading edge. A deformed blade geometries is shown in Fig. 7. The aerodynamic loads at the wind speed of 3.5, 8, 12.5, and 16 m/s were obtained from the CFD simulation.

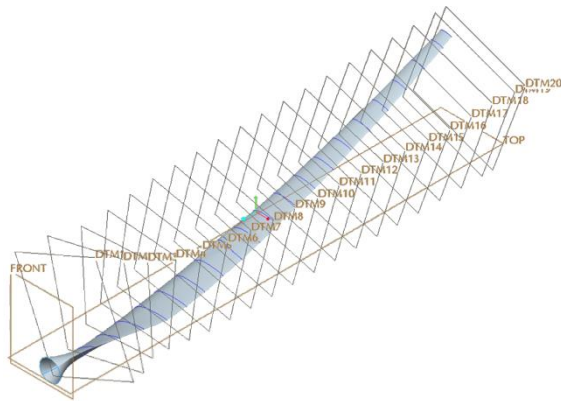


Fig. 7 Deformed blade geometry

The tip deflection of the blades with 3 types of skin layouts is presented in Fig. 8. The deflections resulting from layouts B2 and B3 closely match each other. The maximum different of 5.68% occurs at the wind speed of 16 m/s. The blade with layout B1 is more rigid because it contains higher proportion of 0° layers.

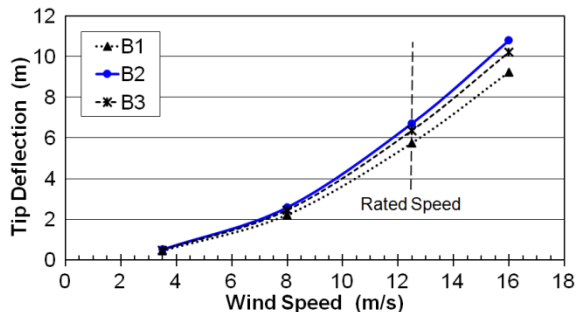


Fig. 8 Blade tip deflection

The twist angle of the blade tip at various wind velocities is shown in Fig. 9. The blade with layout B1 does not have bent-twist coupling. The twist results

are probably due to external forces and moments acting on the blade. The blade with layout B3 twists more than the blade B2, which can be expected from the values of parameter B_t . The average twist angle of the blade B3 at all wind velocities is 1.77 times higher than that of the blade B2.

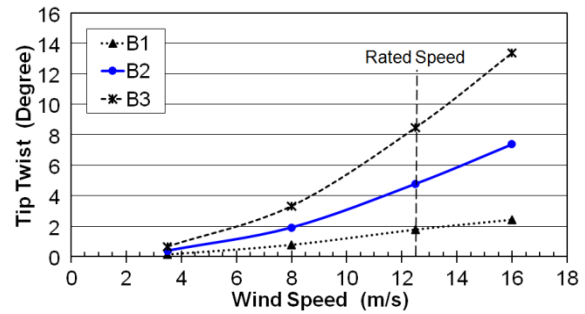


Fig. 9 Blade tip twist

6. BLADE EFFICIENCY

Deformed blade geometries are reproduced for each layout type at each wind speed. In total, 12 blade geometries are obtained from the FEA results. New CFD simulations are then performed on these blades to determine the power coefficients. The deformed geometries should resemble the real blade shapes in operation and thus should be used for efficiency evaluation. The original blade geometry is also retained for power coefficient evaluation. It is treated as a rigid blade that does not deform in any wind speed. The results serve as a baseline for other blades.

Figure 10 presents the power coefficient of the 4 blades. At wind speed 3.5 m/s, the C_p of all blades are comparable. The deformable blades still have very small difference at 8 m/s but their C_p values are noticeably higher than that of the baseline. The blades perform differently at wind speed 12.5 m/s. The C_p of blade B1 does not change much. The C_p of the blade B2 keeps increasing while that of the blade B3 decreases considerably. Since the blades twist toward stall, small twist angles can increase the lift force and efficiency. However, the twist angle of the blade B3 could become too large thus induce flow separation which spoils the lift force and decreases efficiency. At wind speed 16 m/s, the blade B1 does not twist much further and the C_p is practically the same as that of lower speeds. The blades B2 and B3 become noticeably less efficient, likely because of too large twist angles.

From the efficiency standpoint, the blade with layout B2 is suitable for the designed wind speeds. The twist angles are 1.91° at 8 m/s and 4.79° at 12.5 m/s. However, other structural design constraints such as maximum tip deflection, allowable stresses and strains, weight etc must be considered before the blade configuration can be serviceable.

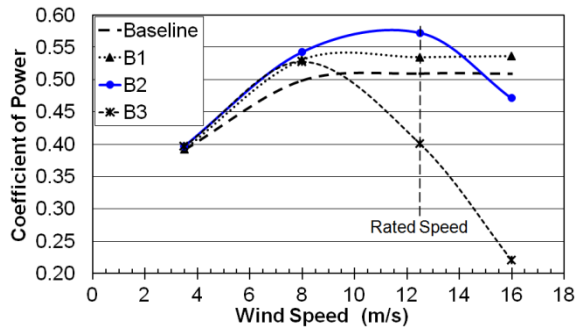


Fig. 10 Coefficient of Power (C_p)

7. CONCLUSION

Coupling deformation is a particular property of composite laminates. Three levels of bend-twist coupling were implemented into a 41.25-meter blade geometry based on GE 1.5 GLX wind turbine. The coupling was produced from the E-Glass/Epoxy blade skins to twist toward stall under bending loads. Aerodynamic loads were obtained from CFD simulation and cross-checked with the analytical BEM theory. The blade structural configuration and the aerodynamic loads were then modeled for finite element analysis. Finally, the deformed geometries of the blades were used to produce new 3D models for the prediction of the coefficient of power (C_p) by CFD.

The blades made from 3 types of layups have similar deflection, vastly different twist, and notably different efficiency. The results show that the deflection has little influence on the power coefficient. On the other hand, the blade twist has strong influence on the power coefficient. Small twist toward stall helps increasing efficiency while too large twist produces flow separation and decrease efficiency.

Simulation of 3D blade models can help designing for a bend-twist coupling suitable to the blade shape and wind speed. Since this is an aeroelastic problem, deformed geometries are assumed to be the blade shapes in operation and should be used to calculate the blade performance. Other structural design constraints must be considered before the blade configuration can be serviceable.

8. REFERENCES

- [1] Lobitz DW, Veers PS, Eisler GR, Laino DJ, Migliore PG, and Bir G, "The use of twist-coupled blades to enhance the performance of horizontal axis wind turbines", Sandia National Laboratory, SAND2001-1303, 2001, 84 p.
- [2] de Goeij WC, van Tooren MJL, and Beukers A, "Implementation of bending-torsion coupling in the design of a wind-turbine rotor-blade", Applied Energy, Vol. 63, 1999, pp. 191-207.
- [3] Locke J and Valencia U, "Design studies for twist-coupled wind turbine blades", Wichita State University, SAND2004-0522, 2004, 127 p.
- [4] Maheri A, Noroozi S, and Vinney J, "Application of combined analytical/FEA coupled aero-structure simulation in design of wind turbine adaptive blades", Renewable Energy, Vol. 32, 2007, pp. 2011-2018.
- [5] Rafiee R, Tahani M, and Moradi M, "Simulation of aeroelastic behavior in a composite wind turbine blade", Journal of Wind Engineering and Industrial Aerodynamics, Vol. 151, 2016, pp.60-69.
- [6] Jones RM, "Mechanics of composite materials". Pennsylvania, USA: Taylor & Francis, Inc., 1999, 519 p.
- [7] Sun CT and Zheng S, "Delamination characteristics of double-cantilever beam and end-notched flexure composite specimens", Composites Science and Technology, Vol. 56, 1996, pp. 451-459.
- [8] Phelps C and Singleton J, "Wind turbine blade design", Cornell University, M.Eng. Report, 2011, 35 p.
- [9] Ingram G, "Wind Turbine Blade Analysis using the Blade Element Momentum Method", Durham University, Note, 2011, 21 p.
- [10] Hepperle M, "Java Foil", www.mh-aerotoools.de/airfoils/javafoil.htm, accessed on 17/6/2015.
- [11] Zuteck M, "Adaptive Blade Concept Assessment: Curved Planform Induced Twist Investigation", Sandia National Laboratory, SAND2002-2996, 2002, 24 p.
- [12] Performance Composite Ltd., "Mechanical Properties of Carbon Fibre Composite Materials, Fibre / Epoxy resin (120°C Cure)", www.performance-composites.org, accessed on 17/6/2015.
- [13] Yeo H, Truong KV, and Ormiston RA, "Assessment of 1-D Versus 3-D Methods for Modeling Rotor Blade Structural Dynamics", in Proc. 51st Structures, Structural Dynamics, and Materials Conf, AIAA/ASME/ASCE/AHS/ASC, 2010, 19 p.

Copyright © Int. J. of GEOMATE. All right reserved, including the making of copies unless permission is obtained from the copyright proprietors.
